THE JOURNAL OF PHYSICAL CHEMISTRY A

Article

Cite This: J. Phys. Chem. A 2019, 123, 764−770

pubs.acs.org/JPCA

Origin of Bath Gas Dependence in Unimolecular Reaction Rates

Akira Matsugi*

National Institute of Advanced Industrial Science and Technology (AIST), 16-1 Onogawa, Tsukuba, Ibaraki 305-8569, Japan

Supporting Information

ABSTRACT: The bath gas dependence of thermal unimolecular reaction rates arises from different rates and efficiencies of collisions between reactant and third-body molecules. This study aims to unravel the mechanistic origin of this dependence based on the classical trajectories of methyl isocyanide (CH_3NC) colliding with 15 different bath gas molecules (CH_3NC, He, Ar, H_2, N_2, CO, CO_2, HCN, NH_3, CH_4, CH_3F, CF_4, C_2H_2, C_2H_4, and C_2H_6). The collision frequencies, energy transfer parameters, and relative third-body efficiencies are evaluated from the trajectory calculations. The relative third-body efficiencies of the studied bath gases are found to be in good agreement with available experimental data. The results indicate that differences in collision frequencies are the primary source of the bath gas dependence of the low-pressure rate constants. The nature of the long-range intermolecular interaction, particularly, its anisotropy, is suggested to play a key role in determining the collision frequency.

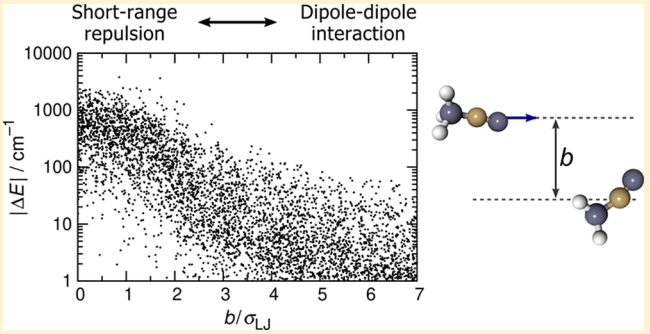

INTRODUCTION

Thermal unimolecular and recombination reaction rates depend on the pressure and composition of the bath gas (or third-body) as the low-pressure kinetics is controlled by collisional energy transfer.[1,2] For unimolecular decomposition and isomerization, the limiting low-pressure rate constant k_0 can be described as a second-order rate constant in the low-pressure regime where the rate constant is proportional to the pressure. The bath gas dependence of the rate constants is represented by relative third-body efficiencies defined as the ratio of k_0 for different bath gases. Various experimental and computational studies[3−16] indicated that the energy transfer process depends on the properties of bath gas molecules such as molecular weight, size, polarizability, and dipole moment. However, the mechanistic origin of the bath gas dependence remains unclear.

The relative third-body efficiency depends on the rate and efficiency of the collisions. In master equations for unimolecular reactions,[1,17] the collisional energy transfer processes are represented by rate coefficients for transitions from energies E' to E by collisions with bath gas molecules, $R(E, E')$. This quantity can be artificially factored into a collision frequency, Z, and a per-collision energy transfer probability function, $P(E, E')$. The latter relates to the weak collision efficiency, β_c.[1,2,18] The value of β_c is recognized to indicate the effectiveness (e.g., whether it is strong or weak) of the third-body collision. The bath gas dependence of k_0 has often been discussed in the context of the relative efficiency of collisions, with the collision frequencies constrained to reference values. The Lennard-Jones (LJ) collision frequency, Z_{LJ}, which is a quantity related to the transport properties of gases, has long been employed as a standard reference.[1,5,7,14,15,19] Several studies[8,9,15] proposed using the capture rate constant for isotropic dispersion interaction, Z_{cap}, which was later shown to be a better quantity for representing the collision frequency for monatomic colliders.[20] While employing reference collision frequencies facilitates comparison of the collision efficiencies (or parameters related to average energy transferred per collision) for different reaction systems, there is no solid justification that these references are consistently appropriate for diverse third-body molecules.

The present study attempts to unravel the mechanistic origin of the bath gas dependence based on classical trajectory calculations. Thermal rate constants for single-channel reactions are not strongly dependent on the detailed shape of $R(E, E')$ or $P(E, E')$[17,21] but can be approximately described by only a few properties of the energy transfer kernel, such as the low-order moments of energy transferred during collisions.[1,20−22] The moments of $R(E, E')$ comprise information relating to both the frequency and efficiency of collisions. As shown in ref 20, the collision frequency and the parameters of $P(E, E')$ can be consistently determined from the energy transfer moments. Here, the method proposed in ref 20 is applied to collisional energy transfer in methyl isocyanide (CH_3NC) colliding with inert bath gas molecules (M). The isomerization of CH_3NC is a classic example of thermal unimolecular reactions, and its rate constants in the falloff and second-order regions have been extensively studied.[3,7,8,23] The relative third-body efficiencies reported for various bath gases[7] provide validation of the classical trajectory method.

Received: November 15, 2018
Revised: January 7, 2019
Published: January 8, 2019

DOI: 10.1021/acs.jpca.8b11081
J. Phys. Chem. A 2019, 123, 764−770

COMPUTATIONAL METHODS

Potential Energy Surface. Classical trajectory calculations were performed for collisions of CH_3NC with 15 bath gas molecules (M = CH_3NC, He, Ar, H_2, N_2, CO, CO_2, HCN, NH_3, CH_4, CH_3F, CF_4, C_2H_2, C_2H_4, and C_2H_6). The trajectories for the monatomic colliders (M = He and Ar) were run on the potential energy surface expressed as $V = V_{molec} + V_{inter}$, where V_{molec} is the CH_3NC intramolecular potential and V_{inter} is the intermolecular interaction potential between CH_3NC and M described below. The intramolecular potential was calculated using the third-order self-consistent charge density functional tight-binding method (DFTB3)[24,25] with the 3OB parameter set.[26,27] For molecular baths, the potential energy surfaces were expressed as $V = V_{full} + V_{corr}$, where V_{full} is the full-dimensional CH_3NC + M potential calculated by the DFTB3 method and V_{corr} is a correction term.

Atom-pairwise functions were used to represent V_{inter} and V_{corr} as

$$V_{inter} = \sum_i V_i(r_i) \tag{1}$$

$$V_i(r) = a_i \exp(-r/b_i) + \sum_{m=6,8} \frac{c_i^{(m)} r_c^m}{r^m + r_c^m} \tag{2}$$

and

$$V_{corr} = \sum_{i,j} V_{ij}(r_{ij}) \tag{3}$$

$$V_{ij}(r) = \sum_{n=1,2} a_{ij}^{(n)} \exp(-r/nr_a) + \sum_{m=6,8,12} \frac{b_{ij}^{(m)} r_b^m}{r^m + r_b^m} \tag{4}$$

where i and j label atoms in CH_3NC and M, respectively, r_i is the internuclear distance between the atom i and M (He or Ar), r_{ij} is the internuclear distance between atoms i and j, $r_a = a_0$ ($a_0 \approx 5.29177 \times 10^{-11}$ m; the Bohr radius), $r_b = r_c = 2a_0$, and a_i, b_i, $c_i^{(m)}$, $a_{ij}^{(n)}$, and $b_{ij}^{(m)}$ are parameters. The parameters were obtained by fitting the interaction energies (ΔV; defined as V relative to that at an infinite separation between CH_3NC and M) to the reference interaction energies (ΔV_{ref}) calculated at the CCSD-(T)-F12/aug-cc-pVDZ level of theory[28,29] for various intramolecular structures, relative orientations, and center-of-mass distances between CH_3NC and M. For each M, 50 different orientations were randomly generated, and the center-of-mass distances were varied from 10 to typically 1−4 Å for each orientation to sample both the repulsive and attractive parts of the interaction potential. The intramolecular structures of CH_3NC and M were generated following the procedure described below. The fittings were performed by a weighted least-squares method, with the weights defined as $w = E_w/(E_w + \Delta V_{ref})$ if $\Delta V_{ref} > 0$ and $w = 1$ otherwise, where $E_w = 10$ kJ mol^{-1}. The fitted parameters are listed in Tables S1 and S2 in the Supporting Information. The mean absolute deviations between ΔV and ΔV_{ref} for $\Delta V_{ref} < 20$ kJ mol^{-1} were in the range of 0.48−0.96 kJ mol^{-1} depending on M.

The DFTB3 and coupled cluster calculations were performed with the DFTB+[30] and Molpro[31] programs, respectively. In the DFTB3 calculations, the tolerance for the self-consistent charge calculation was set to be 10^{-10} to improve the energy convergence in the trajectory integrations.

Classical Trajectory. On the potential energy surfaces described above, 3000−5000 trajectories were run for each M at temperature T = 554 K.[7] The method and procedure for the trajectory calculations are similar to those used in ref 20. The initial vibrational states of CH_3NC were generated by classical microcanonical sampling[20,32] with a fixed vibrational energy E_{vib} of 160 kJ mol^{-1}, which is close to the barrier height for the isomerization.[23] Then, the angular momentum was given from a thermal distribution at temperature T by quasi-classical rigid-rotor sampling.[20,32] For molecular colliders, the initial rovibrational states were generated from thermal distributions at temperature T by employing a quasi-classical normal-mode/rigid-rotor sampling method.[32] The relative velocities of the molecule and collider were determined from the relative translational energy sampled from a thermal distribution. Impact parameter b was uniformly sampled over the range 0−b_{max}. The maximum impact parameter b_{max} was set to be $15a_0$ for M = He, $20a_0$ for Ar, H_2, and N_2, $25a_0$ for CH_4, $30a_0$ for CO, C_2H_2, C_2H_4, and C_2H_6, $35a_0$ for CO_2, $40a_0$ for NH_3 and CF_4, $50a_0$ for HCN and CH_3F, and $60a_0$ for CH_3NC. The convergences with respect to b_{max} were ensured by confirming that the results remained unchanged within the statistical uncertainties when the value of b_{max} was reduced by $5a_0$ from the original value. The initial and final separations between the center of mass of CH_3NC and M were set at $x_0 = 1.5b_{max}$. The collision frequency of trajectories, Z_{traj}, is defined as the hard-sphere collision frequency for a collision diameter b_{max} as

$$Z_{traj} = \pi b_{max}^2 \sqrt{8k_B T/\pi\mu} \tag{5}$$

where k_B is the Boltzmann constant and μ is the reduced mass of CH_3NC and M. The trajectories were propagated using the five-stage, fourth-order symplectic integrator[33] with a time step of 0.2 fs. The total energy was typically conserved to within much less than 1 cm^{-1} during each trajectory.

The downward energy transfer moments of the probability distribution, $\langle \Delta E_d{}^n \rangle_{traj}$, and the quantity $\langle \Delta E_d \ln \Delta E_d \rangle_{traj}$ were obtained from the trajectory calculations as

$$\langle \Delta E_d{}^n \rangle_{traj} = \frac{1}{N_d} \sum_{i=1}^{N_d} w_i (E_i' - E_i)^n \tag{6}$$

and

$$\langle \Delta E_d \ln \Delta E_d \rangle_{traj} = \frac{1}{N_d} \sum_{i=1}^{N_d} w_i (E_i' - E_i) \ln(E_i' - E_i) \tag{7}$$

respectively, where n is the order of the moment, E_i' and E_i are the pre- and postcollision rovibrational energies of the CH_3NC molecule, respectively, for the ith deactivating trajectory, and N_d is the number of trajectories leading to deactivation ($E_i' > E_i$). The weighting factor, $w_i = 2b_i/b_{max}$, corrects for bias in the sampling of impact parameter b. All error limits reported for the parameters derived from the trajectory calculation correspond to two standard errors.

RESULTS AND DISCUSSION

Trajectory Results and Energy Transfer Model. The trajectory calculations revealed that the features of intermolecular energy transfer differ according on the type of colliding molecules. The difference is illustrated in Figure 1, where the absolute values of the energy transferred, $|E - E'|$, are plotted as a function of the impact parameter, b, normalized by the LJ diameter parameter, σ_{LJ}, for M = N_2 and CH_3NC. The vertical dotted lines indicate the effective collision diameters of the LJ

DOI: 10.1021/acs.jpca.8b11081
J. Phys. Chem. A 2019, 123, 764−770

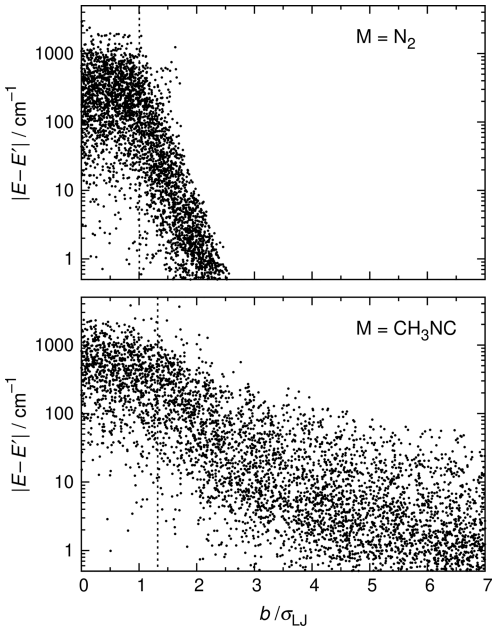

Figure 1. Absolute values of energy transferred in collisions of CH_3NC with N_2 (top) and CH_3NC (bottom) as a function of b/σ_{LJ}. The vertical dotted lines indicate the effective collision diameters of the LJ collision frequencies (see the text).

collision frequencies, which are drawn at $b/\sigma_{LJ} = (\Omega^{(2,2)*})^{1/2}$, where $\Omega^{(2,2)*}$ is the reduced collision integral involved in Z_{LJ} as

$$Z_{LJ} = \pi\sigma_{LJ}^{\ 2}\sqrt{8k_BT/\pi\mu}\,\Omega^{(2,2)*} \tag{8}$$

The LJ parameters, σ_{LJ} and ε_{LJ}, were estimated by combining rules (arithmetic mean for σ_{LJ} and geometric mean for ε_{LJ}) from the pure gas values[7,34] listed in Table 1. The reduced collision

Table 1. Pure Gas Values of the LJ Diameter (σ) and Well Depth (ε) Parameters[7,34] and Dipole Moments (μ)[37]

M	σ (Å)	ε/k_B (K)	μ (D)
CH_3NC	4.47	380	3.85
He	2.551	10.22	
Ar	3.542	93.3	
H_2	2.827	59.7	
N_2	3.798	71.4	
CO	3.690	91.7	0.112
CO_2	3.941	195.2	
HCN	3.63	569.1	2.98
NH_3	2.90	558.3	1.47
CH_4	3.758	148.6	
CH_3F	3.73	333	1.85
CF_4	4.662	134	
C_2H_2	4.033	231.8	
C_2H_4	4.163	224.7	
C_2H_6	4.443	215.7	

integrals $\Omega^{(2,2)*}$ for nonpolar colliders were calculated from the LJ (12−6) potential, while the angle-averaged reduced collision integrals based on the Stockmayer (12−6−3) potential[35,36] were employed for polar colliders using the dipole moments[37] listed in Table 1. These integrals were calculated by interpolating the tabulated values.[35] Figure 1 shows that the amount of energy transferred in a collision with N_2 decreases sharply in the range of $1 < b/\sigma_{LJ} < 2$ due to the weakened intermolecular interaction at large impact parameters. On the other hand, considerable energy transfer can occur even at b/σ_{LJ} much larger than $(\Omega^{(2,2)*})^{1/2}$ for M = CH_3NC. This latter example indicates the inability of Z_{LJ} to represent the collision frequency for energy transfer processes.

The adequacy of the collision frequency for describing the energy transfer process can be evaluated from the energy transfer moments.[20] Figure 2 plots the moments of $R(E, E')$ for

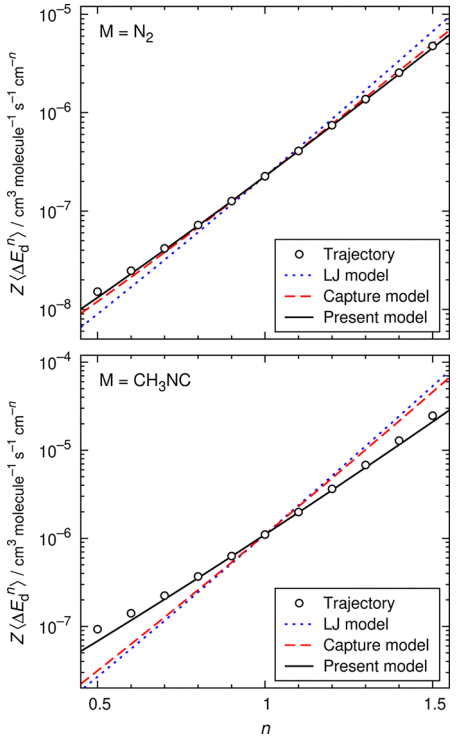

Figure 2. Comparisons of the trajectory-based moments (circles; $Z_{traj}\langle\Delta E_d^{\ n}\rangle_{traj}$) with the moments $Z\langle\Delta E_d^{\ n}\rangle$ of the LJ model (dotted lines), the capture model (dashed lines), and the present model (solid lines) for collisions of CH_3NC with N_2 (top) and CH_3NC (bottom).

deactivating ($E < E'$) collisions, $Z\langle\Delta E_d^{\ n}\rangle$, as a function of the order n (including noninteger order) near the first-order for M = N_2 and CH_3NC. The moments for a given distribution function are given by

$$Z\langle\Delta E_d^{\ n}\rangle = Z\frac{\int_0^{E'}(E'-E)^nP(E,E')\,dE}{\int_0^{E'}P(E,E')\,dE} \tag{9}$$

where the functional form of $P(E, E')$ for deactivating collisions used in the present study is the exponential-down model[1]

$$P(E,E') \propto \exp\left(-\frac{E'-E}{\alpha}\right) \tag{10}$$

where α is the parameter corresponding to the average energy transferred in deactivating collisions, $\langle\Delta E_d\rangle$. One way to determine the value of α is to scale the first-order moment of trajectories by using a reference collision frequency.[15,22] As in the previous study,[20] using Z_{LJ} as the reference ("LJ model" in Figure 2) led to steeper n dependence of the moment than that for the trajectory results. Another reference is the capture rate constant for dispersion interaction[20]

DOI: 10.1021/acs.jpca.8b11081
J. Phys. Chem. A 2019, 123, 764−770

Table 2. Calculated Energy Transfer Parameters, Collision Frequencies, and $Z\beta_c$

M	α (cm^{-1})	Z (10^{-10} cm^3 $molecule^{-1}$ s^{-1})	$Z\beta_c$ (10^{-10} cm^3 $molecule^{-1}$ s^{-1})
CH_3NC	206 ± 27	53.6 ± 4.2	4.60 ± 0.58
He	178 ± 18	10.6 ± 0.6	0.736 ± 0.089
Ar	213 ± 21	7.02 ± 0.44	0.633 ± 0.076
H_2	162 ± 23	19.3 ± 1.7	1.17 ± 0.18
N_2	229 ± 22	9.87 ± 0.62	0.981 ± 0.113
CO	150 ± 18	19.0 ± 1.3	1.02 ± 0.15
CO_2	194 ± 22	22.5 ± 1.3	1.76 ± 0.23
HCN	179 ± 26	38.2 ± 3.4	2.68 ± 0.41
NH_3	281 ± 31	24.5 ± 1.3	3.20 ± 0.37
CH_4	238 ± 23	18.0 ± 1.1	1.89 ± 0.20
CH_3F	169 ± 27	42.0 ± 3.9	2.72 ± 0.46
CF_4	207 ± 27	19.3 ± 1.3	1.68 ± 0.25
C_2H_2	222 ± 26	20.7 ± 1.3	1.97 ± 0.27
C_2H_4	288 ± 38	17.4 ± 1.4	2.35 ± 0.32
C_2H_6	310 ± 31	18.1 ± 1.0	2.67 ± 0.29

$$Z_{cap} = 2\Gamma(2/3)(k_B T/\varepsilon_{LJ})^{-1/3}\pi\sigma_{LJ}^{\ 2}\sqrt{8k_B T/\pi\mu} \quad (11)$$

where Γ is the gamma function. This reference ("Capture model" in Figure 2) gave an improved result for M = N_2 but still failed to reproduce the n dependence of the trajectory-based moments for M = CH_3NC. In the latter case, the intermolecular interaction at large separations may be dominated by the dipole−dipole interaction; however, the contribution of the dipole−dipole interaction to the capture rate constant is only significant at very low temperatures.[38]

The first-order moment, $Z\langle\Delta E_d\rangle$, and the derivative of the moment with respect to n at $n = 1$, $Z\langle\Delta E_d \ln \Delta E_d\rangle$, were found to be important quantities for describing low-pressure kinetics[20] (the higher-order moments are also important for multichannel reactions[39] but not for single-channel reactions[20] as in the present case). The parameter α and collision frequency Z can be evaluated from these quantities obtained from the trajectory calculations as[20]

$$\ln\alpha = \frac{\langle\Delta E_d \ln \Delta E_d\rangle_{traj}}{\langle\Delta E_d\rangle_{traj}} - \psi(2) \quad (12)$$

$$Z = Z_{traj}\frac{\langle\Delta E_d\rangle_{traj}}{\alpha} \quad (13)$$

where ψ is the di-gamma function defined as $\psi(x) = \Gamma'(x)/\Gamma(x)$. Figure 2 shows that the moments of the trajectories and their n dependence near first-order are correctly reproduced by employing Z and α calculated using the present method.

Relative Third-Body Efficiencies. The results of the trajectory calculations are validated against the experimental relative third-body efficiencies,[7] $k_0(M)/k_0(M_{ref})$, where $k_0(M)$ represents the limiting low-pressure rate constant for bath gas M and reference bath gas M_{ref} (=CH_3NC). As k_0 depends on the product of Z and β_c, the relative third-body efficiency was calculated as the ratio of $Z\beta_c$ for M to that for M_{ref}. In this study, β_c is defined for any collision frequency Z and corresponds to $\beta_{c\Delta E}$ of Troe's notation.[18] The approximate expression given by Troe[18] was used to calculate β_c as

$$\beta_c \approx \left(\frac{\alpha}{\alpha + F_E k_B T}\right)^2 \quad (14)$$

where F_E is the energy dependence factor of the density of states, which was calculated to be $F_E = 1.29$ for the reaction threshold energy of 160 kJ mol^{-1} by employing the rigid-rotor harmonic-oscillator approximations. Although the reaction threshold could be smaller than this because of the tunneling, the relative third-body efficiencies are almost unchanged (deviating by less than 3%) even if the value of F_E is raised to be 1.52 (equivalent to halving the reaction threshold energy). The calculated values of α, Z, and $Z\beta_c$ are listed in Table 2. The calculated relative third-body efficiencies are found to be consistent with the experimental data within the statistical uncertainties, as indicated in the top panel of Figure 3, which demonstrates the ability of the classical trajectory method.

The energy transferred per collision is not strongly dependent on third-body M, as indicated in the bottom panel of Figure 3. The parameter α, which corresponds to $\langle\Delta E_d\rangle$, has similar values of ~200 cm^{-1} for the studied bath gas molecules except for NH_3, C_2H_4, and C_2H_6, for which α is close to 300 cm^{-1}. These values are smaller than $k_B T$ (385 cm^{-1} at 554 K); therefore, unlike the early thoughts,[7] all of the molecules studied herein can be regarded as weak colliders with $\beta_c < 0.2$. No clear correlation between k_0 and β_c is recognized from Figure 3. Consequently, the bath gas dependence of k_0 primarily originates from the difference in the collision frequency.

The collision frequencies obtained from the trajectory calculations depend strongly on the nature of the bath gas molecules. These are plotted and compared with Z_{LJ} and Z_{cap} in Figure 3. For all of the molecules studied, the calculated collision frequencies are higher than Z_{LJ} by factors ranging from 1.8 (M = Ar) to 6.7 (M = CH_3F). In accordance with the previous study on the collisions of nonpolar molecules with monatomic colliders,[20] the collision frequencies for M = He, Ar, H_2, and N_2 are close to the capture rate constants. On the other hand, some of the other polyatomic colliders, especially those with large permanent dipole moments (M = CH_3NC, HCN, and CH_3F), have substantially higher collision frequencies, which support their relatively large third-body efficiencies.

Role of Intermolecular Forces. The results presented above suggest the roles of the attractive and repulsive intermolecular forces in characterizing the collisional energy transfer processes. The coincidence between the trajectory-based collision frequencies and capture rate constants for the monatomic and homonuclear diatomic colliders proposes that the energy transfer effectively occurs through repulsive interactions.[20] For these colliders, the long-range interaction is dominated by the nearly isotropic dispersion force so that the

DOI: 10.1021/acs.jpca.8b11081
J. Phys. Chem. A 2019, 123, 764−770

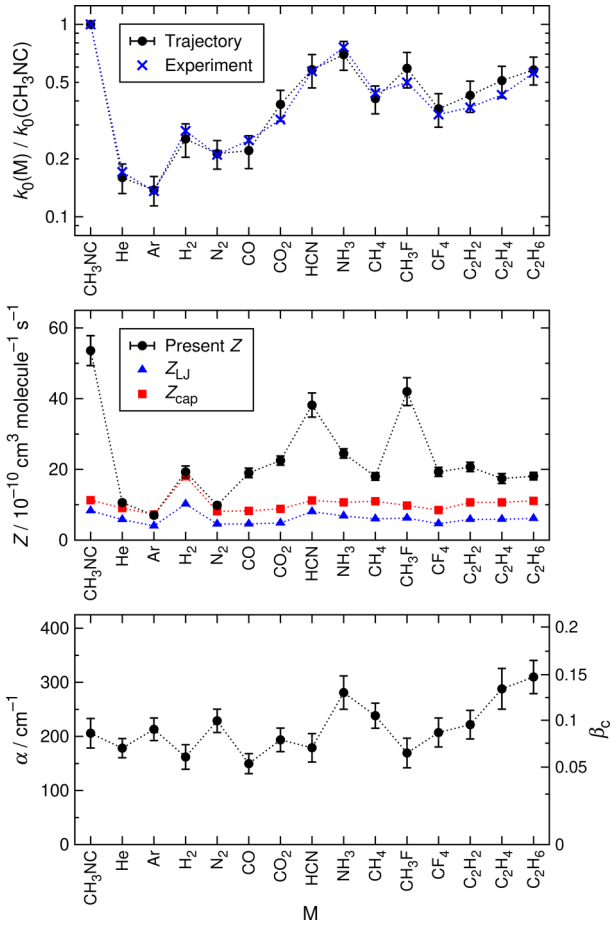

Figure 3. Relative third-body efficiencies for the CH_3NC isomerization at 554 K (top; the experimental data are taken from ref 7), the calculated collision frequencies Z plotted together with Z_{LJ} and Z_{cap} for comparison (middle), and the calculated energy transfer parameters α and corresponding values of the collision efficiency β_c (bottom) for the different bath gases. The error bars indicate the statistical uncertainties (two standard errors) of the trajectory calculations.

repulsive part of the potential can be reached if the trajectory is captured by the attractive force. In contrast, the dipole−dipole interaction is anisotropic and dependent on the rotational orientation of the dipoles; the intermolecular force between two polar molecules can be both attractive and repulsive even at large intermolecular separations. The high collision frequencies calculated for the polar colliders are potentially explained by energy transfer taking place at the repulsive regions of the dipole−dipole interactions. Moreover, even for nonpolar polyatomic colliders, anisotropy of the intermolecular interaction can be induced by properties such as structural anisotropy, nonrigidity, polarizability, and multipole moments of the collider molecule. The importance of the long-range interaction in the energy transfer process was also highlighted before.[7]

To examine the importance of the anisotropy, orientation dependences of the intermolecular interaction potentials between CH_3NC and M were evaluated. For each M, 4000 different intramolecular structures of CH_3NC and M were generated with the same method as that used for generating the initial geometries of the trajectories. The interaction potentials between the two molecules were calculated at fixed center-of-mass distances, r_{com}, of $2\sigma_{LJ}$, $3\sigma_{LJ}$, and $4\sigma_{LJ}$ with random relative orientations. The standard deviation of the interaction potentials at the center-of-mass distance r_{com}, $s(r_{com})$, is given as

$$s(r_{com}) = \left[\frac{1}{N}\sum_{i=1}^{N}(\Delta V_i(r_{com}) - \Delta\bar{V}(r_{com}))^2\right]^{1/2} \quad (15)$$

where i labels the number of samples N (= 4000), $\Delta V_i(r_{com})$ is the ith interaction potential at the center-of-mass distance r_{com}, and $\Delta\bar{V}(r_{com})$ is the average

$$\Delta\bar{V}(r_{com}) = \frac{1}{N}\sum_{i=1}^{N}\Delta V_i(r_{com}) \quad (16)$$

With a sample size of N = 4000, the calculated standard deviation $s(r_{com})$ converged to within 4% at the 95% confidence level. Here, this standard deviation is used as a measure of the anisotropy of intermolecular interaction.

A good correlation was found between the collision frequencies and the standard deviations of the interaction potentials. Figure 4 shows the calculated $s(r_{com})$ at the three

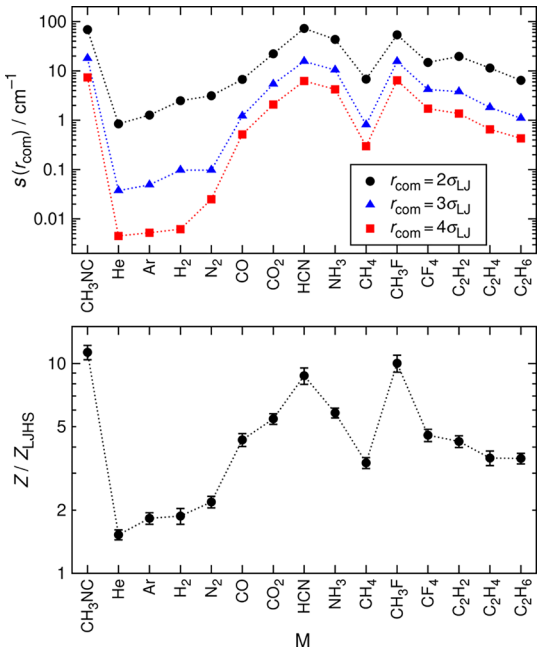

Figure 4. Comparisons of the standard deviations of the interaction potentials $s(r_{com})$ at $r_{com} = 2\sigma_{LJ}$, $3\sigma_{LJ}$, and $4\sigma_{LJ}$ (top) and calculated collision frequencies Z normalized by Z_{LJHS} (bottom).

different r_{com} values. As expected, the polar colliders show strong anisotropy while the interactions with the monatomic and homonuclear diatomic colliders are nearly isotropic. Even a small dipole moment of CO causes discernible differences in $s(r_{com})$ when compared with those of N_2. The relatively large $s(r_{com})$ for nonpolar CO_2 may arise from anisotropy of its molecular structure; the same can be said for M = C_2H_2 in comparisons with C_2H_4 and C_2H_6. For tetrahedral CH_4 and CF_4, the nonrigidity of the molecules should be responsible for the anisotropy in the interactions. The large electronegativity of fluorine atoms in CF_4 can induce fluctuation of the interaction energies as the molecule vibrates, which potentially explains the larger $s(r_{com})$ for M = CF_4 than that for CH_4 especially at large separations. These trends observed in $s(r_{com})$ also hold in the collision frequency. The calculated collision frequencies

DOI: 10.1021/acs.jpca.8b11081
J. Phys. Chem. A 2019, 123, 764−770

normalized by the hard-sphere collision frequency for the diameter σ_{LJ}, Z_{LJHS}, defined by

$$Z_{LJHS} = \pi\sigma_{LJ}^{2}\sqrt{8k_BT/\pi\mu} \quad (17)$$

are plotted in the bottom panel of Figure 4. The normalization by Z_{LJHS} is intended to facilitate the comparison of Z by excluding the effects of molecular weight and size. The bath gas dependence of Z closely resembles that of $s(r_{com})$. The correlation coefficients between $\ln(Z/Z_{LJHS})$ and $\ln(s(r_{com}))$ are 0.97, 0.96, and 0.95 for $r_{com} = 2\sigma_{LJ}$, $3\sigma_{LJ}$, and $4\sigma_{LJ}$, respectively. Therefore, the anisotropy of the intermolecular interaction controls the collision frequency for energy transfer in collisions with polyatomic molecules.

CONCLUSIONS

The energy transfer processes of methyl isocyanide colliding with 15 different bath gas molecules are investigated by classical trajectory calculations. The energy transfer parameters and collision frequencies for the exponential-down model are evaluated from the trajectory-based energy transfer moments. The calculated relative third-body efficiencies for the thermal isomerization of methyl isocyanide in the studied bath gases are in good agreement with the experimental data available in the literature. The present analysis leads to the following conclusions:

(i) The average energy transferred in deactivating collisions, $\langle\Delta E_d\rangle$, is consistently smaller than k_BT for all of the bath gas molecules studied. The strong collision assumption[23] appears to be invalid even for highly polar molecules.

(ii) The difference in the collision frequency, rather than the collision efficiency per collision (or $\langle\Delta E_d\rangle$), is primarily responsible for the bath gas dependence of the unimolecular reaction rates at low pressures.

(iii) While intermolecular energy transfer takes place at the repulsive regions of the interaction potential, the nature of the long-range interaction is of importance in determining the collision frequency. In line with the conclusion drawn in the previous study,[20] the collision frequency can be represented by the capture rate constants if the long-range interaction is dominated by isotropic forces. For general polyatomic colliders, the collision frequency correlates with the anisotropy of the long-range interaction potential.

ASSOCIATED CONTENT

Supporting Information

The Supporting Information is available free of charge on the ACS Publications website at DOI: 10.1021/acs.jpca.8b11081.

Tables listing the fitted potential parameters (PDF)

AUTHOR INFORMATION

Corresponding Author

*E-mail: a.matsugi@aist.go.jp.

ORCID

Akira Matsugi: 0000-0001-5789-7208

Notes

The author declares no competing financial interest.

ACKNOWLEDGMENTS

This work was supported in part by JSPS KAKENHI Grant Number 18K13709.

REFERENCES

(1) Gilbert, R. G.; Smith, S. C. *Theory of Unimolecular and Recombination Reactions*; Blackwell: Oxford, 1990.

(2) Holbrook, K. A.; Pilling, M. J.; Robertson, S. H. *Unimolecular Reactions*, 2nd ed.; Wiley: Chichester, 1996.

(3) Tardy, D. C.; Rabinovitch, B. S. Intermolecular Vibrational Energy Transfer in Thermal Unimolecular Systems. *Chem. Rev.* **1977**, *77*, 369−408.

(4) Oref, I.; Tardy, D. C. Energy Transfer in Highly Excited Large Polyatomic Molecules. *Chem. Rev.* **1990**, *90*, 1407−1445.

(5) Volpe, M.; Johnston, H. S. Energy Transfer Processes in the Unimolecular Decomposition of Nitryl Chloride1. *J. Am. Chem. Soc.* **1956**, *78*, 3903−3910.

(6) Fletcher, F. J.; Rabinovitch, B. S.; Watkins, K. W.; Locker, D. J. Energy Transfer in Thermal Methyl Isocyanide Isomerization. Experimental Survey. *J. Phys. Chem.* **1966**, *70*, 2823−2833.

(7) Chan, S. C.; Rabinovitch, B. S.; Bryant, J. T.; Spicer, L. D.; Fujimoto, T.; Lin, Y. N.; Pavlou, S. P. Energy Transfer in Thermal Methyl Isocyanide Isomerization. Comprehensive Investigation. *J. Phys. Chem.* **1970**, *74*, 3160−3176.

(8) Michael, J. V.; Su, M.-C.; Sutherland, J. W.; Carroll, J. J.; Wagner, A. F. Rate Constants for H + O_2 + M → HO_2 + M in Seven Bath Gases. *J. Phys. Chem. A* **2002**, *106*, 5297−5313.

(9) Fernandes, R. X.; Luther, K.; Troe, J.; Ushakov, V. G. Experimental and Modelling Study of the Recombination Reaction H + O_2 (+M) → HO_2 (+M) between 300 and 900 K, 1.5 and 950 bar, and in the Bath Gases M = He, Ar, and N_2. *Phys. Chem. Chem. Phys.* **2008**, *10*, 4313−4321.

(10) Lim, K. F.; Gilbert, R. G. Trajectory Simulations of Collisional Energy Transfer of Highly Vibrationally Excited Azulene. *J. Phys. Chem.* **1990**, *94*, 77−84.

(11) Lendvay, G.; Schatz, G. C. Choice of Gas Kinetic Rate Coefficients in the Vibrational Relaxation of Highly Excited Polyatomic Molecules. *J. Phys. Chem.* **1992**, *96*, 3752−3756.

(12) Lendvay, G.; Schatz, G. C. Trajectory Studies of Collisional Relaxation of Highly Excited CS_2 by H_2, CO, HCl, CS_2, and CH_4. *J. Chem. Phys.* **1992**, *96*, 4356−4365.

(13) Ming, L.; Sewell, T. D.; Nordholm, S. A Simulation Study of Energy Transfer in Methyl Isocyanide-Inert Gas Collisions. *Chem. Phys.* **1995**, *199*, 83−104.

(14) Jasper, A. W.; Miller, J. A. Theoretical Unimolecular Kinetics for CH_4 + M ⇄ CH_3 + H + M in Eight Baths, M = He, Ne, Ar, Kr, H_2, N_2, CO, and CH_4. *J. Phys. Chem. A* **2011**, *115*, 6438−6455.

(15) Jasper, A. W.; Miller, J. A.; Klippenstein, S. J. Collision Efficiency of Water in the Unimolecular Reaction CH_4 (+H_2O) ⇄ CH_3 + H (+H_2O): One-Dimensional and Two-Dimensional Solutions of the Low-Pressure-Limit Master Equation. *J. Phys. Chem. A* **2013**, *117*, 12243−12255.

(16) Jasper, A. W.; Oana, C. M.; Miller, J. A. Third-Body" Collision Efficiencies for Combustion Modeling: Hydrocarbons in Atomic and Diatomic Baths. *Proc. Combust. Inst.* **2015**, *35*, 197−204.

(17) Miller, J. A.; Klippenstein, S. J.; Raffy, C. Solution of Some One- and Two-Dimensional Master Equation Models for Thermal Dissociation: The Dissociation of Methane in the Low-Pressure Limit. *J. Phys. Chem. A* **2002**, *106*, 4904−4913.

(18) Troe, J. Theory of Thermal Unimolecular Reactions at Low Pressures. I. Solutions of the Master Equation. *J. Chem. Phys.* **1977**, *66*, 4745−4757.

(19) Troe, J. Predictive Possibilities of Unimolecular Rate Theory. *J. Phys. Chem.* **1979**, *83*, 114−126.

(20) Matsugi, A. Collision Frequency for Energy Transfer in Unimolecular Reactions. *J. Phys. Chem. A* **2018**, *122*, 1972−1985.

(21) Lim, K. F.; Gilbert, R. G. Calculation of Collisional-Energy-Transfer Rates in Highly Excited Molecules. *J. Phys. Chem.* **1990**, *94*, 72−77.
(22) Brown, N. J.; Miller, J. A. Collisional Energy Transfer in the Low-Pressure-Limit Unimolecular Dissociation of HO_2. *J. Chem. Phys.* **1984**, *80*, 5568−5580.
(23) Schneider, F. W.; Rabinovitch, B. S. The Thermal Unimolecular Isomerization of Methyl Isocyanide. Fall-Off Behavior. *J. Am. Chem. Soc.* **1962**, *84*, 4215−4230.
(24) Elstner, M.; Porezag, D.; Jungnickel, G.; Elsner, J.; Haugk, M.; Frauenheim, T.; Suhai, S.; Seifert, G. Self-Consistent-Charge Density-Functional Tight-Binding Method for Simulations of Complex Materials Properties. *Phys. Rev. B: Condens. Matter Mater. Phys.* **1998**, *58*, 7260−7268.
(25) Gaus, M.; Cui, Q.; Elstner, M. DFTB3: Extension of the Self-Consistent-Charge Density-Functional Tight-Binding Method (SCC-DFTB). *J. Chem. Theory Comput.* **2011**, *7*, 931−948.
(26) Gaus, M.; Goez, A.; Elstner, M. Parametrization and Benchmark of DFTB3 for Organic Molecules. *J. Chem. Theory Comput.* **2013**, *9*, 338−354.
(27) Kubillus, M.; Kubař, T.; Gaus, M.; Řezáč, J.; Elstner, M. Parameterization of the DFTB3Method for Br, Ca, Cl, F, I, K, and Na in Organic and Biological Systems. *J. Chem. Theory Comput.* **2015**, *11*, 332−342.
(28) Adler, T. B.; Knizia, G.; Werner, H.-J. A Simple and Efficient CCSD(T)-F12 Approximation. *J. Chem. Phys.* **2007**, *127*, 221106.
(29) Knizia, G.; Adler, T. B.; Werner, H.-J. Simplified CCSD(T)-F12 Methods: Theory and Benchmarks. *J. Chem. Phys.* **2009**, *130*, 054104.
(30) Aradi, B.; Hourahine, B.; Frauenheim, T. DFTB+, a Sparse Matrix-Based Implementation of the DFTB Method. *J. Phys. Chem. A* **2007**, *111*, 5678−5684.
(31) Werner, H.-J.; Knowles, P. J.; Knizia, G.; Manby, F. R.; Schutz, M.; et al. *MOLPRO version 2012.1, a package of ab initio programs*; University College Cardiff Consultants Limited: Cardiff, U.K., 2012.
(32) Peslherbe, G. H.; Wang, H.; Hase, W. L. Monte Carlo Sampling for Classical Trajectory Simulations. *Adv. Chem. Phys.* **2007**, *105*, 171−201.
(33) Gray, S. K.; Noid, D. W.; Sumpter, B. G. Symplectic Integrators for Large Scale Molecular Dynamics Simulations: A Comparison of Several Explicit Methods. *J. Chem. Phys.* **1994**, *101*, 4062−4072.
(34) Poling, B. E.; Prausnitz, J. M.; O'Connell, J. P. *The Properties of Gases and Liquids*, 5th ed.; McGraw-Hill Professional: Boston, MA, 2001.
(35) Monchick, L.; Mason, E. A. Transport Properties of Polar Gases. *J. Chem. Phys.* **1961**, *35*, 1676−1697.
(36) Mason, E. A.; Monchick, L. Transport Properties of Polar-Gas Mixtures. *J. Chem. Phys.* **1962**, *36*, 2746−2757.
(37) Nelson, R. D., Jr.; Lide, D. R.; Maryott, A. A. *Selected Values of Electric Dipole Moments for Molecules in the Gas Phase*, National Standard Reference Data Series; National Bureau of Standards, NSRDS-NBS10, 1967.
(38) Georgievskii, Y.; Klippenstein, S. J. Long-Range Transition State Theory. *J. Chem. Phys.* **2005**, *122*, 194103.
(39) Matsugi, A. Dissociation Channels, Collisional Energy Transfer, and Multichannel Coupling Effects in the Thermal Decomposition of CH_3F. *Phys. Chem. Chem. Phys.* **2018**, *20*, 15128−15138.

DOI: 10.1021/acs.jpca.8b11081
J. Phys. Chem. A 2019, 123, 764−770